Ultrathin Plasmonic Tungsten Oxide Quantum Wells with Controllable Free Carrier Densities

Gyanaranjan Prusty,[1,#] Jacob T. Lee,[1,#] Soenke Seifert,[2] Barry B. Muhoberac,[1] and Rajesh Sardar*[,1,3]

[1]Department of Chemistry and Chemical Biology, Indiana University-Purdue University Indianapolis, 402 N. Blackford Street, Indianapolis, Indiana 46202, United States

[2]X-ray Science Division, Argonne National Laboratory, Argonne, Illinois 60439, United States

[3]Integrated Nanosystems Development Institute, Indiana University-Purdue University Indianapolis, 423 W. Michigan Street, Indianapolis, Indiana 46202, United States

Supporting Information Placeholder

ABSTRACT: Localized surface plasmon resonances (LSPR) of nanostructures can be tuned by controlling their morphology, local dielectric environment, and free carrier concentration. We report the colloidal synthesis of ~3 tungsten-oxygen (W-O) layer thick (~1 nm), two-dimensional (2D) WO_{3-x} nanoplatelets (NPLs) (x ~ 0.55 – 1.03), which display tunable near-infrared LSPR spectra and high free electron density (N_e). This high N_e arises predominantly from the large shape factor of 2D NPLs. Importantly, the W to O composition ratios inferred from the LSPR measurements of NPLs show much higher percentage of oxygen vacancies than those determined by X-ray diffraction analysis, suggesting that the shape factor and aspect ratio of ultrathin WO_{3-x} NPLs are the key to producing an unprecedentedly larger N_e, although synthesis temperature is also an independent factor. We find that NPL formation is kinetically controlled, whereas manipulation of thermodynamic parameters leads to N_e as high as 4.13 X 10^{22} cm^{-3}, which is in close proximity to that of plasmonic noble metals, and thus our oxide-based nanostructures can be considered as *quasi-metallic*. The unique structural properties of 2D nanomaterials along with the high N_e of WO_{3-x} NPLs provide an attractive alternative to plasmonic noble metal nanostructures for various plasmon-driven energy conversion schemes, and design of flexible photochromic nanodevices.

Impressively, the discovery of atomically-thin graphene[1-2] has completely transformed much material science research involving two-dimensional (2D) nanostructures. By deconvoluting fundamental structure-composition-property relationships, novel electronic and charge transport properties have been created with 2D transition metal dichalcogenides, metal chalcogenides, MXenes, and perovskite nanostructures to meet the high demand in advanced solid-state device fabrication.[3-4] By altering the chemical compositions and/or physical characteristics of nanostructures, new optoelectronic properties emerge that are not achievable with their bulk counterparts. Among many exotic properties, localized surface plasmon resonance (LSPR),[5] which originates from the collective oscillation of surface bound charges upon interaction with incident light, is unique, because these plasmon charges, either electrons or holes, can be utilized in photovoltaic, photocatalytic, and photothermal therapy applications, as well as bio- and molecular sensing.[6-13]

The LSPR properties of nanostructures are mostly controlled by free carrier densities that depend on the size, shape, and dielectric medium around them.[7, 14] Discovery of high free carrier densities (10^{22} -10^{23} cm^{-3}) of plasmonic metals such as Au and Ag led to the exploration of their LSPR properties, which resulted in tremendous progress in various aspects of nanoscience and nanotechnology research. Beside plasmonic metals, doped metal oxides (e.g., In_2O_3, Al_2O_3, CdO, ZnO, etc.)[15-19] also display LSPR properties, which can be modulated by controlling their dopant concentrations.[20] The desirable dispersion relationships[21-22] of 2D plasmonic nanostructures along with excellent charge transport abilities make them attractive candidates for various optoelectronic-based applications. Herein, we report the observation of the LSPR properties of colloidally-synthesized, ultrathin (~3-W-O layer thick) tungsten oxide quantum wells[23] in the shape of nanoplatelets (NPLs) that can be tuned over 1200-1800 nm in the near-infrared (NIR) spectrum. We chose tungsten oxide to synthesize ultrathin NPLs because this composition has an unmatched potential to display high-temperature superconductivity, fast ion transport, and extremely large magnetoresistance that together lead to various applications such as smart windows, spintronics, quantum computing, and energy storage.[24]

In this communication, tungsten oxide NPLs were synthesized colloidally from the oxidative decomposition of

tungsten (V) ethoxide in the presence of myristic acid (MA) and oleylamine (OLA) at 270 ^{O}C. Transmission electron microscopy (TEM) analysis of the purified product, which produces a dark blue colloidal solution in carbon tetrachloride (CCl_4), shows the formation of platelet-type structures with 21.2 and 7.0 nm length and width, respectively (see **Figure 1A &B**, and **Figure S1)**. The geometry of these NPLs resembles metal chalcogenide NPLs.[25] We measured the thickness of tungsten oxide NPLs by Guinier analysis of small angle X-ray scattering (SAXS) spectrum which yields ~1 nm (**Figure 1C**). We also calculated the thickness of NPLs from the TEM analysis and determined it to be 1.0 ± 0.2 nm, see **Figure S2**. The structural characterization provides an aspect ratio (width-to-thickness) of 7.0. As illustrated in **Figure 1D**, X-ray diffraction (XRD) analysis of NPLs confirms monoclinic lattice structure with predicted composition of $W_{18}O_{49}$, which is a stoichiometric of $WO_{2.72}$.[26]

It is important to mention that due to broad XRD peak of ultrathin NPLs, it is difficult to absolutely determine the precise stoichiometry of our LSPR active tungsten oxides NPLs. As shown previously,[27-28] LSPR-based calculations using complex dielectric function for plasmonic materials can provide a nearly quantitative stoichiometric ratio of plasmonic nanostructures. We determined that the calculated stoichiometry of tungsten oxide NPLs is much different than the XRD-derived value, as discussed below. Therefore, we refer to our synthesized NPLs as WO_{3-x}. Considering each W-O layer as 0.37 nm thick, our isolated tungsten oxide NPLs contain ~3 such layers. **Table S1** lists specific reaction conditions for the synthesis of WO_{3-x} NPLs. Although, one-dimensional (1D) nanostructures such as nanorods and nanowires composed of $WO_{2.72}$ have been reported in the literature,[29-31] to our knowledge, this is first example of the synthesis of 2D NPLs consisting of different stoichiometric states of inorganic lattice composition. It must be pointed out that the detailed investigation of the LSPR properties of previously reported 1D nanostructures is also lacking.

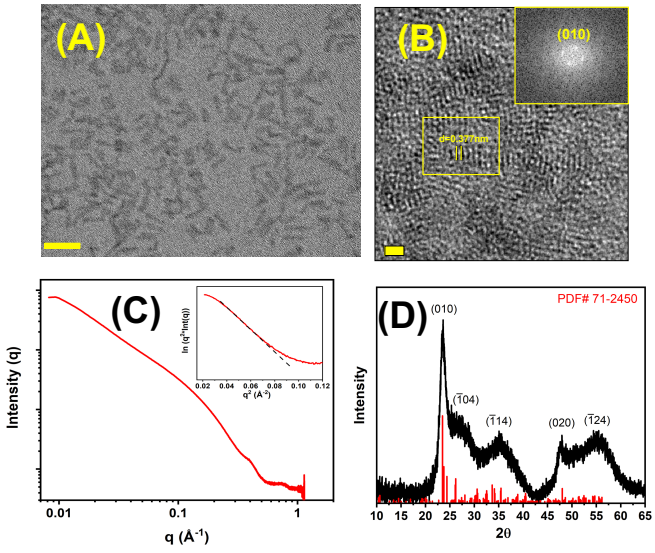

Figure 1. (A) Low and (B) high-resolution TEM images of WO_{3-x} NPLs. The scale bars in (A) and (B) are 10 and 5 nm, respectively. The inset in (B) shows FFT of (010) plane. The yellow box shows *d-spacing* of 0.377 nm. (C) SAXS spectrum and (D) XRD pattern of NPLs. The inset in (C) shows Guinier fit to determine the thickness.

Notably, as shown in **Figure 2A**, WO_{3-x} NPLs exhibit a remarkably well-defined, characteristic LSPR peak (λ_{LSPR}) at ~1470 nm. To confirm that this NIR optical response of WO_{3-x} NPLs arises from LSPR due to oxygen vacancies in the WO_{3-x} crystal lattice that generate electrons as free carriers, and not from scattering, impurities, or absorption by local defects,[28, 32] we examined the NIR absorption band position as a function of solvent refractive index (bulk refractive index). The λ_{LSPR} red shifts as refractive indices of solvents increases (**Figure 2B and Figure S3**). This direction is in agreement with nanostructures that display LSPR properties.[5] Our WO_{3-x} NPLs show an LSPR sensitivity of 330 nm/refractive index unit (nm/RIU), which is higher than previously reported for $WO_{2.83}$ nanorods (280 nm/RIU)[24] and Cs_xWO_3 nanostructures (188 nm/RIU),[32] and is comparable to 2D plasmonic metal nanostructures.[7, 33]

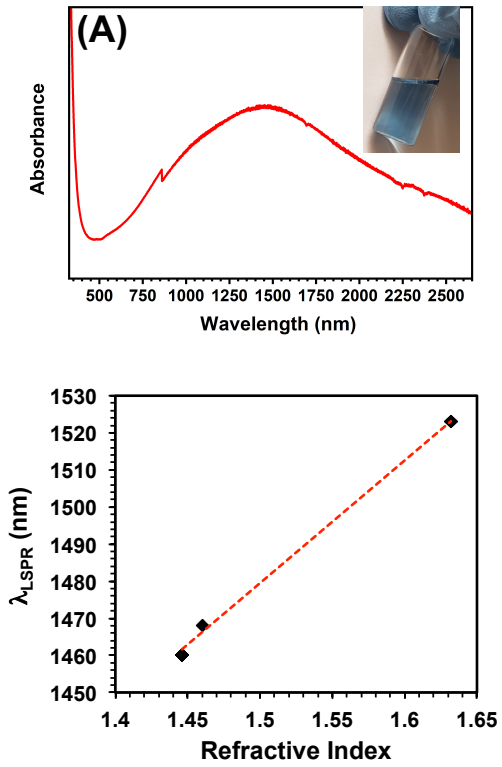

Figure 2. (A) UV-Vis-NIR spectrum of WO_{3-x} NPLs in CCl_4. The inset shows photograph of WO_{3-x} NPLs in $CHCl_3$. (B) The dependence of λ_{LSPR} maximum on the index of refraction of solvent (330 nm/RIU).

This relatively higher RIU sensitivity of our plasmonic WO_{3-x} NPLs in comparison to other tungsten oxide-based nanostructures is due to the larger shape factor, κ, of 2D nanostructures as compared to their 1D counterparts.[34] It should be noted that the polarizability of plasmonic charge carriers at the nanostructure-solvent medium interface is much greater when κ is higher (see **Table S2**). Under such conditions, a minute dielectric change in the surrounding medium would significantly alter the LSPR properties.[34]

Moreover, ultrathin edges and sharp corners of WO_{3-x} NPLs are expected to contain a high density of free carriers, which should produce a large near-field enhancement of surface plasmon,[35] and thus results in a large LSPR response, as demonstrated for 2D Au[8, 10, 33] and Ag nanoprisms.[7, 36] Our, spectroscopic characterizations (^{1}H NMR and FTIR) confirm both MA and OLA acting as surface passivating ligands (**Figure S4 &S5**). Due to the presence of oxygen containing surface passivating ligands, it is difficult to determine the W to O composition ratios by other techniques, such as X-ray photoelectron spectroscopy or electron paramagnetic resonance spectroscopy. Perhaps, a Drude treatment of the dielectric function could be the only method to precisely determine the stoichiometry of WO_{3-x} NPLs.

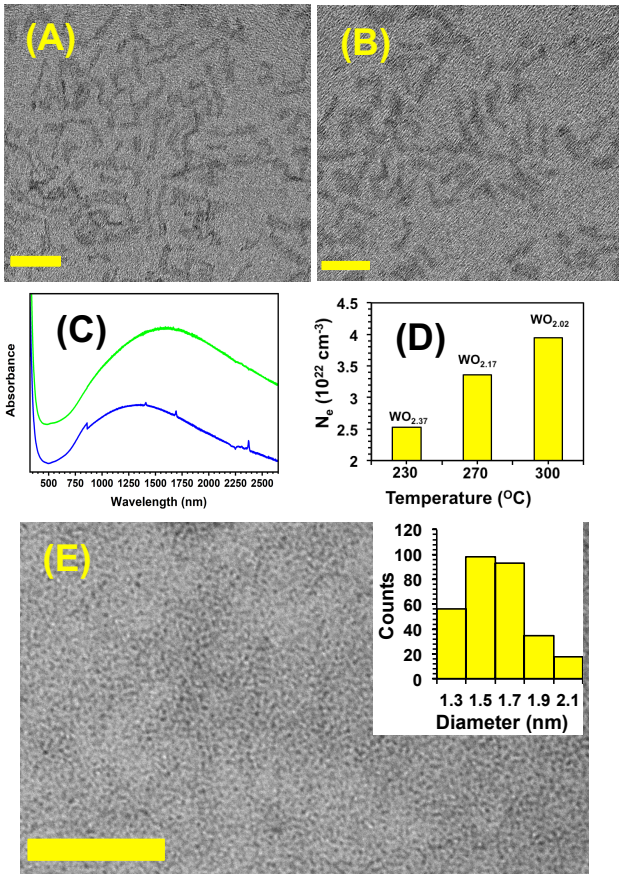

Figure 3. HRTEM images of $WO_{2.72}$ NPLs in CCl_4 synthesized at (A) 230 and (B) 300 ^{O}C. Scale bars are 20 nm. (C) UV-Vis-NIR spectrum of WO_{3-x} NPLs in CCl_4 synthesized at (green) 230 and (blue) 300 ^{O}C. (D) The plot of free carrier densities of WO_{3-x} NPLs versus reaction temperature. (E) A representative TEM image of spherical WO_{3-x} NCs. The scale bar is 50 nm. The inset shows a histogram of the size distribution. The calculated composition of WO_{3-x} NPLs synthesized at 230, 270, and 300 ^{O}C are $WO_{2.37}$, $WO_{2.17}$, and $WO_{2.02}$, respectively.

The λ_{LSPR} of WO_{3-x} NPLs is expected to depend on the size, shape and dielectric constant of the inorganic core, as well as the dielectric constant of the surrounding medium. Combining our experimentally determined λ_{LSPR} energy with the Drude model for bulk materials, we can calculate free electron density (N_e). Eq. 1 represents the relation used between LSPR frequency (ω_{LSPR}) and bulk plasma oscillation frequency of electrons (ω_p) for tungsten oxide with a high frequency dielectric constant (ϵ_∞) of 4.5.

$$\omega_{LSPR} = \sqrt{\frac{\omega_p^2}{\epsilon_\infty - \varepsilon_r} - \gamma^2} \quad (1)$$

Where ε_r denotes the real part of the complex dielectric function, ε, of the plasmonic nanostructures.

$$\varepsilon_r = -\kappa\varepsilon_m \quad (2)$$

Here ε_m is the dielectric constant of the surrounding medium, which we have taken as the bulk refractive index (CCl_4 = 2.24). The electrons of the nanostructure oscillate due to the incident electromagnetic field, and the motion is collisionally damped with a bulk collision frequency γ, 0.736 eV, see **Table S1**. Finally, ω_p depends on N_e as

$$\omega_p^2 = \frac{N_e e^2}{\varepsilon_o m_e} \quad (3)$$

where, m_e is the effective mass of an electron and ε_0 is the permittivity of free space. As provided by literature for WO_{3-x} we used $m_e = 1.2\ m_0$,[26] where m_0 is the rest mass of an electron. With the assumption of the WO_{3-x} NPL as oblate spheroids with an aspect ratio of 7.0 (shape factor of 9.6) and based on the above-mentioned values, we calculate N_e to be 3.36 X 10^{22} cm^{-3}. This value is nearly five-fold higher than the stoichiometrically determined N_e value for $WO_{2.83}$ nanorods (N_e = 6.3 X 10^{21} cm^{-3}),[24] and is more than two order of magnitude higher than 2D metal chalcogenide nanodisks (N_e = 1.0 X 10^{20} cm^{-3}).[27, 37] With the assumption that two electrons in the WO_{3-x} crystal lattice originate from a fully ionized oxygen deficiency and by utilizing the LSPR properties of WO_{3-x} NPLs, we determine the oxygen deficiency as 27.7%, which provides the stoichiometric composition of NPLs as $WO_{2.17}$ (see **Table S2)**. Therefore, the calculated stoichiometric state of the NPL lattice shows more oxygen deficiency than the predicted value by the XRD analysis. This could possibly be the reason underlying the unprecedentedly high free carrier densities of our synthesized WO_{3-x} NPLs. We should also mention that the calculated oxygen deficiency, and hence the stoichiometric state of the NPL lattice could be slightly overestimated because of the intrinsic and inhomogeneous line-broadening that arises from shape dispersion, as previously reported for LSPR active metal chalcogenide nanocrystals.[28] Additionally, inter-NPL plasmonic coupling was not considered in the N_e calculation.

Despite tremendous promise, controlling LSPR properties of tungsten oxide-based nanostructures in the NIR region has yet to be achieved.[24, 38] A predictive way to modulate the LSPR properties would be to synthesize differently-shaped nanostructures because it is well known that the LSPR properties of nanostructures strongly depend on their size and shape.[7, 20] Therefore, we investigated the ability of temperature to manipulate the thermodynamic growth regime and prepare anisotropically-shaped WO_{3-x} nanostructures.[39-40] To our surprise, WO_{3-x} NPLs of a few atomic layers thickness are also formed when the reaction was carried out at 230 and 300 ^{O}C (**Figure 3A-B and Table**

S1). NPLs synthesized at both temperatures display a monoclinic crystal structure (**Figure S6 & S7**).

Importantly, the λ_{LSPR} blue shifts with increasing reaction temperature (**Figure 3C**). The N_e values of WO_{3-x} NPLs that were synthesized at 300 and 230 ^{O}C are calculated to be 3.95 X 10^{22} and 2.53 X 10^{22} cm^{-3}, respectively (see **Figure 3D)**, which correspond to $WO_{2.02}$ and $WO_{2.37}$ stoichiometric compositions. The larger N_e of $WO_{2.00}$ NPLs synthesized at 300 ^{O}C is close to that of plasmonic metals, and thus our nanostructures can be considered as *"quasi-metallic"*.[41] The application of a large shape factor of ultrathin WO_{3-x} NPLs, which also depends on the aspect ratio of the nanostructures, can only lead to λ_{LSPR} blue shifts at a fixed N_e because the shape factor and N_e are independent parameters modulating the optoelectronic properties of NPLs. A more acceptable explanation for unprecedentedly large N_e of WO_{3-x} NPLs is their ultrathin shape in which a large percentage of oxygen atoms are expected to reside on the surface and at the sharp corners and edges. These atoms are expected to be highly susceptible to undergoing fast ionization at high temperature, creating more oxygen vacancies and thus dramatically increasing the free carrier concentrations. It is well known in the literature for plasmonic noble metal nanostructures that λ_{LSPR} red shifts as the aspect ratio increases.[33-34, 36] Based on our calculations, WO_{3-x} NPLs synthesized at 300 ^{O}C should display the most red-shifted λ_{LSPR} because of its the highest aspect ratio. However, we observe an opposite LSPR effects (see **Table S1**). In contrast, Eq. 2 and 3 suggest that with an increase N_e, the λ_{LSPR} should blue shift, which we observe here. Therefore, for LSPR-active metal oxide nanostructures, both the shape factor and collision frequency must be carefully taken into consideration in order to generalize the LSPR-related properties. Nevertheless, to the best of our knowledge, this is the highest N_e value reported for LSPR-active metal oxide nanostructures including recently reported spherical ReO_3 NCs.[42] Finally, we estimated the direct optical band gap of WO_{3-x} NPLs from a plot of $(\alpha h\nu)^2$ versus $h\nu$ (Tauc plot). We observe a monotonic increase in the band gap energy with increasing reaction temperature (**Figure S8**) that can be attributed to the Burstein-Moss shift.[43] The band gap energy is also in agreement with increasing N_e value for NPLs, which were synthesized at a different temperature.

We also investigated the effects of surface passivating ligands controlling the kinetic growth regime at a particular temperature[39-40, 44] on the shape/size of the nanostructure formed, and thus the N_e of tungsten oxide nanostructures. We determine that at 270 ^{O}C: (1) The presence of both long hydrocarbon chain amines and acids together in the reaction mixture is a prerequisite to produce WO_{3-x} NPLs. (2) The formation of tungsten oxide nanostructures is not observed when the reaction is carried out in the presence of OLA alone with no acid. (3) Nearly monodispersed, spherical, monoclinic WO_{3-x} NCs are formed (**Figure 3E and S9**) when the synthesis is conducted in the presence of just MA as the surface passivating ligand. Supporting information **Table S1 and S2** contains reaction conditions, morphology, and dimensions of tungsten oxide nanostructures, and representative N_e values. Based on the experimentally determined λ_{LSPR} of ~985 nm for average 1.6 nm diameter WO_{3-x} NCs, we calculate a N_e value of 2.68 X 10^{22} cm^{-3}. This is not only higher than ReO_3 NCs (1.57 X 10^{22} cm^{-3}),[42] but also tungsten-based nanostructures provide additional benefits as compared to metal-oxide nanostructures containing rhenium, which is a rare earth metal and very expensive.

Based on the experimental results, our hypothesis is that the first step in NPL formation is that spherical NCs are passivated with aliphatic carboxylate ligands as a binding head group to form tungsten-carboxylates. A bilayer structure is formed between the aliphatic chains of amine and acid ligands through van der Waals (vdW) interactions.[45-46] Particularly, vdW interactions and chain interdigitation induce entropically controlled mesoscale growth in which individual spherical, WO_{3-x} NCs fuse together and transform into NPLs (**Figure 3**). This hypothesis is supported by the appearance of a mixture of spherical NCs and NPLs in the presence of lower concentrations of OLA in the reaction mixture (**Figure S10**). These low concentrations may not provide adequate vdW interactions to convert all the spherical NCs into NPLs. The vdW attraction between bulky long aliphatic chain ligands should lead to the formation of lamellar[47] NPL structures and prevent fusion of individual NPLs (see Scanning-TEM images in **Figure S2)**. Additional UV-Vis-NIR spectra, TEM images, and histograms for different ligands are provided in the Supporting Information File (**Figure S11-14**). Detailed time-dependent microscopic and spectroscopic characterizations will be required to precisely determine the growth mechanism of WO_{3-x} NPLs and this is an ongoing research focus of our laboratory.

In conclusion, we have demonstrated the colloidal synthesis of ~1 nm thick WO_{3-x} NPLs with N_e value as high as 4.13 X 10^{22} cm^{-3} (**Table S2**). We have observed that the reaction temperature plays a significant role in manipulating the oxygen vacancies, which control the overall N_e values. Importantly, the band-gap of WO_{3-x} NPLs can be tuned by manipulating the N_e values without changing the crystal stoichiometry. We have also determined that the presence of long-chain aliphatic amines in the reaction mixture is a prerequisite for the formation of NPLs. We believe that vdW interactions between the aliphatic carbon chains induces mesoscale growth of spherical NCs into a NPL shape. Together, our research has the unique potential to expand scientific research in the following areas: (1) The LSPR properties of WO_{3-x} NPLs along with their high surface area should facilitate applications involving light harvesting schemes such as photovoltaics and photocatalysis.[11-13] (2) Tungsten oxide is capable of displaying electrochromic properties, which should enhance the efficiency of smart windows and antiglare automobile rear-view mirrors.[11, 13, 48] (3) Finally, due to low electronic heat capacities of metal oxide nanostructures in general, hot electrons with higher energies, as compared to traditional plasmonic noble metal nanostructures, can be generated. This optoelectronic property is extremely beneficial for plasmon-assisted photo-thermal therapy.[49]

ASSOCIATED CONTENT

Supporting Information. Materials and methods, experimental details, additional TEM images, histograms, UV-vis-NIR, XRD, SAXS, NMR and FTIR spectra, and a table.

AUTHORS CONTRIBUTION

G.P and J.T.L. contributed equally to this work.

AUTHOR INFORMATION

Corresponding Author

rsardar@iupui.edu

Notes

The authors declare no competing financial interest

ACKNOWLEDGMENT

Financial support was provided by NSF (DMR-1747582). This research used resources of the Advanced Photon Source, a U.S. Department of Energy (DOE) User Facility operated for the DOE Office of Science by Argonne National Laboratory under Contract DEAC02-06CH11357. TEM analyses were conducted at the Electron Microscopy Core Facility, Indiana University School of Medicine.

REFERENCES

1. Geim, A. K.; Novoselov, K. S., The rise of graphene. *Nat. Mater.* **2007,** *6* (3), 183-191.
2. Novoselov, K. S.; Geim, A. K.; Morozov, S. V.; Jiang, D.; Zhang, Y.; Dubonos, S. V.; Grigorieva, I. V.; Firsov, A. A., Electric Field Effect in Atomically Thin Carbon Films. *Science* **2004,** *306* (5696), 666-669.
3. Nasilowski, M.; Mahler, B.; Lhuillier, E.; Ithurria, S.; Dubertret, B., Two-Dimensional Colloidal Nanocrystals. *Chem. Rev.* **2016,** *116* (18), 10934-10982.
4. Tan, C.; Cao, X.; Wu, X.-J.; He, Q.; Yang, J.; Zhang, X.; Chen, J.; Zhao, W.; Han, S.; Nam, G.-H.; Sindoro, M.; Zhang, H., Recent Advances in Ultrathin Two-Dimensional Nanomaterials. *Chem. Rev.* **2017,** *117* (9), 6225-6331.
5. Mulvaney, P., Surface Plasmon Spectroscopy of Nanosized Metal Particles. *Langmuir* **1996,** *12* (3), 788-800.
6. Joshi, G. K.; Deitz-McElyea, S.; Liyanage, T.; Lawrence, K.; Mali, S.; Sardar, R.; Korc, M., Label-Free Nanoplasmonic-Based Short Noncoding RNA Sensing at Attomolar Concentrations Allows for Quantitative and Highly Specific Assay of MicroRNA-10b in Biological Fluids and Circulating Exosomes. *ACS Nano* **2015,** *9* (11), 11075-11089.
7. Mayer, K. M.; Hafner, J. H., Localized Surface Plasmon Resonance Sensors. *Chem. Rev.* **2011,** *111* (6), 3828-3857.
8. Joshi, G. K.; Blodgett, K. N.; Muhoberac, B. B.; Johnson, M. A.; Smith, K. A.; Sardar, R., Ultrasensitive Photoreversible Molecular Sensors of Azobenzene-Functionalized Plasmonic Nanoantennas. *Nano Lett.* **2014,** *14* (2), 532-540.
9. Joshi, G. K.; Deitz-McElyea, S.; Johnson, M.; Mali, S.; Korc, M.; Sardar, R., Highly Specific Plasmonic Biosensors for Ultrasensitive MicroRNA Detection in Plasma from Pancreatic Cancer Patients. *Nano Lett.* **2014,** *14* (12), 6955-6963.
10. Liyanage, T.; Nagaraju, M.; Johnson, M.; Muhoberac, B. B.; Sardar, R., Reversible Tuning of the Plasmoelectric Effect in Noble Metal Nanostructures Through Manipulation of Organic Ligand Energy Levels. *Nano Lett.* **2019,** *20*, 192-200.
11. Atwater, H. A.; Polman, A., Plasmonics for improved photovoltaic devices. *Nat. Mater.* **2010,** *9* (3), 205-213.
12. Linic, S.; Christopher, P.; Ingram, D. B., Plasmonic-metal nanostructures for efficient conversion of solar to chemical energy. *Nat. Mater.* **2011,** *10* (12), 911-921.
13. Zhou, L.; Swearer, D. F.; Zhang, C.; Robatjazi, H.; Zhao, H.; Henderson, L.; Dong, L.; Christopher, P.; Carter, E. A.; Nordlander, P.; Halas, N. J., Quantifying hot carrier and thermal contributions in plasmonic photocatalysis. *Science* **2018,** *362* (6410), 69-72.
14. Halas, N. J.; Lal, S.; Chang, W.-S.; Link, S.; Nordlander, P., Plasmons in Strongly Coupled Metallic Nanostructures. *Chem. Rev.* **2011,** *111* (6), 3913-3961.
15. Kanehara, M.; Koike, H.; Yoshinaga, T.; Teranishi, T., Indium tin oxide nanoparticles with compositionally tunable surface plasmon resonance frequencies in the near-IR region. *J. Am. Chem. Soc.* **2009,** *131* (49), 17736-7.
16. Schimpf, A. M.; Lounis, S. D.; Runnerstrom, E. L.; Milliron, D. J.; Gamelin, D. R., Redox Chemistries and Plasmon Energies of Photodoped In2O3 and Sn-Doped In2O3 (ITO) Nanocrystals. *J. Am. Chem. Soc.* **2015,** *137* (1), 518-524.
17. Ye, X.; Fei, J.; Diroll, B. T.; Paik, T.; Murray, C. B., Expanding the spectral tunability of plasmonic resonances in doped metal-oxide nanocrystals through cooperative cation-anion codoping. *J. Am. Chem. Soc.* **2014,** *136* (33), 11680-6.
18. Faucheaux, J. A.; Jain, P. K., Plasmons in Photocharged ZnO Nanocrystals Revealing the Nature of Charge Dynamics. *J. Phys. Chem. Lett.* **2013,** *4* (18), 3024-3030.
19. Gordon, T. R.; Paik, T.; Klein, D. R.; Naik, G. V.; Caglayan, H.; Boltasseva, A.; Murray, C. B., Shape-dependent plasmonic response and directed self-assembly in a new semiconductor building block, indium-doped cadmium oxide (ICO). *Nano Lett.* **2013,** *13* (6), 2857-63.
20. Agrawal, A.; Cho, S. H.; Zandi, O.; Ghosh, S.; Johns, R. W.; Milliron, D. J., Localized Surface Plasmon Resonance in Semiconductor Nanocrystals. *Chem. Rev.* **2018,** *118* (6), 3121-3207.
21. Wang, Y.; Ou, J. Z.; Chrimes, A. F.; Carey, B. J.; Daeneke, T.; Alsaif, M. M. Y. A.; Mortazavi, M.; Zhuiykov, S.; Medhekar, N.; Bhaskaran, M.; Friend, J. R.; Strano, M. S.; Kalantar-Zadeh, K., Plasmon Resonances of Highly Doped Two-Dimensional MoS2. *Nano. Lett.* **2015,** *15* (2), 883-890.
22. Scholz, A.; Stauber, T.; Schliemann, J., Plasmons and screening in a monolayer of MoS${}_{2}$. *Phys. Rev. B* **2013,** *88* (3), 035135.
23. Pelton, M.; Ithurria, S.; Schaller, R. D.; Dolzhnikov, D. S.; Talapin, D. V., Carrier Cooling in Colloidal Quantum Wells. *Nano Lett.* **2012,** *12* (12), 6158-6163.
24. Manthiram, K.; Alivisatos, A. P., Tunable localized surface plasmon resonances in tungsten oxide nanocrystals. *J. Am. Chem. Soc.* **2012,** *134* (9), 3995-8.
25. Ithurria, S.; Dubertret, B., Quasi 2D Colloidal CdSe Platelets with Thicknesses Controlled at the Atomic Level. *J. Am. Chem. Soc.* **2008,** *130* (49), 16504-16505.
26. Molenda, J.; Kubik, A., Electrical Properties of Nonstoichiometric WO3−y at Temperatures 77 to 300 K. *phys. status solidi b* **1995,** *191* (2), 471-478.
27. Hsu, S. W.; On, K.; Tao, A. R., Localized surface plasmon resonances of anisotropic semiconductor nanocrystals. *J. Am. Chem. Soc.* **2011,** *133* (47), 19072-5.
28. Luther, J. M.; Jain, P. K.; Ewers, T.; Alivisatos, A. P., Localized surface plasmon resonances arising from free carriers in doped quantum dots. *Nat. Mater.* **2011,** *10* (5), 361-6.
29. Liu, J.; Margeat, O.; Dachraoui, W.; Liu, X.; Fahlman, M.; Ackermann, J., Gram-Scale Synthesis of Ultrathin Tungsten Oxide Nanowires and their Aspect Ratio-Dependent Photocatalytic Activity. *Adv. Func. Mater.* **2014,** *24* (38), 6029-6037.
30. Yella, A.; Tahir, M. N.; Meuer, S.; Zentel, R.; Berger, R.; Panthöfer, M.; Tremel, W., Synthesis, Characterization, and Hierarchical Organization of Tungsten Oxide Nanorods: Spreading Driven by Marangoni Flow. *J. Am. Chem. Soc.* **2009,** *131* (48), 17566-17575.
31. Heo, S.; Kim, J.; Ong, G. K.; Milliron, D. J., Template-Free Mesoporous Electrochromic Films on Flexible Substrates from Tungsten Oxide Nanorods. *Nano Lett.* **2017,** *17* (9), 5756-5761.

32. Mattox, T. M.; Bergerud, A.; Agrawal, A.; Milliron, D. J., Influence of Shape on the Surface Plasmon Resonance of Tungsten Bronze Nanocrystals. *Chem. Mater.* **2014,** *26* (5), 1779-1784.
33. Joshi, G. K.; McClory, P. J.; Muhoberac, B. B.; Kumbhar, A.; Smith, K. A.; Sardar, R., Designing Efficient Localized Surface Plasmon Resonance-Based Sensing Platforms: Optimization of Sensor Response by Controlling the Edge Length of Gold Nanoprisms. *J. Phys. Chem. C* **2012,** *116* (39), 20990-21000.
34. Jain, P. K.; El-Sayed, M. A., Surface Plasmon Resonance Sensitivity of Metal Nanostructures: Physical Basis and Universal Scaling in Metal Nanoshells. *J. Phys. Chem. C* **2007,** *111* (47), 17451-17454.
35. Kim, J.; Agrawal, A.; Krieg, F.; Bergerud, A.; Milliron, D. J., The Interplay of Shape and Crystalline Anisotropies in Plasmonic Semiconductor Nanocrystals. *Nano Lett.* **2016,** *16* (6), 3879-3884.
36. Khan, A. U.; Zhao, S.; Liu, G., Key Parameter Controlling the Sensitivity of Plasmonic Metal Nanoparticles: Aspect Ratio. *J. Phys. Chem. C* **2016,** *120* (34), 19353-19364.
37. Liu, M.; Xue, X.; Ghosh, C.; Liu, X.; Liu, Y.; Furlani, E. P.; Swihart, M. T.; Prasad, P. N., Room-Temperature Synthesis of Covellite Nanoplatelets with Broadly Tunable Localized Surface Plasmon Resonance. *Chem. Mater.* **2015,** *27* (7), 2584-2590.
38. Lee, K.; Seo, W. S.; Park, J. T., Synthesis and Optical Properties of Colloidal Tungsten Oxide Nanorods. *J. Am. Chem. Soc.* **2003,** *125* (12), 3408-3409.
39. Jun, Y.-w.; Choi, J.-s.; Cheon, J., Shape Control of Semiconductor and Metal Oxide Nanocrystals through Nonhydrolytic Colloidal Routes. *Angew. Chem. Int. Ed.* **2006,** *45* (21), 3414-3439.
40. Xia, Y.; Xia, X.; Peng, H.-C., Shape-Controlled Synthesis of Colloidal Metal Nanocrystals: Thermodynamic versus Kinetic Products. *J. Am. Chem. Soc.* **2015,** *137* (25), 7947-7966.
41. Hoffman, A. J.; Alekseyev, L.; Howard, S. S.; Franz, K. J.; Wasserman, D.; Podolskiy, V. A.; Narimanov, E. E.; Sivco, D. L.; Gmachl, C., Negative refraction in semiconductor metamaterials. *Nat. Mater.* **2007,** *6* (12), 946-950.
42. Ghosh, S.; Lu, H.-C.; Cho, S. H.; Maruvada, T.; Price, M. C.; Milliron, D. J., Colloidal ReO3 Nanocrystals: Extra Re d-Electron Instigating a Plasmonic Response. *J. Am. Chem. Soc.* **2019,** *141* (41), 16331-16343.
43. Burstein, E., Anomalous Optical Absorption Limit in InSb. *Phys. Rev.* **1954,** *93* (3), 632-633.
44. Yin, Y.; Alivisatos, A. P., Colloidal nanocrystal synthesis and the organic-inorganic interface. *Nature* **2005,** *437* (7059), 664-70.
45. Cölfen, H.; Mann, S., Higher-Order Organization by Mesoscale Self-Assembly and Transformation of Hybrid Nanostructures. *Angew. Chem. Int. Ed.* **2003,** *42* (21), 2350-2365.
46. Teunis, M. B.; Johnson, M. A.; Muhoberac, B. B.; Seifert, S.; Sardar, R., Programmable Colloidal Approach to Hierarchical Structures of Methylammonium Lead Bromide Perovskite Nanocrystals with Bright Photoluminescent Properties. *Chem. Mater.* **2017,** *29* (8), 3526-3537.
47. Son, J. S.; Wen, X.-D.; Joo, J.; Chae, J.; Baek, S.-i.; Park, K.; Kim, J. H.; An, K.; Yu, J. H.; Kwon, S. G.; Choi, S.-H.; Wang, Z.; Kim, Y.-W.; Kuk, Y.; Hoffmann, R.; Hyeon, T., Large-Scale Soft Colloidal Template Synthesis of 1.4 nm Thick CdSe Nanosheets. *Angew. Chem. Int. Ed.* **2009,** *48* (37), 6861-6864.
48. Chavez, S.; Aslam, U.; Linic, S., Design Principles for Directing Energy and Energetic Charge Flow in Multicomponent Plasmonic Nanostructures. *ACS Energy Lett.* **2018,** *3* (7), 1590-1596.
49. Gibbs, S. L.; Staller, C. M.; Milliron, D. J., Surface Depletion Layers in Plasmonic Metal Oxide Nanocrystals. *Acc. Chem. Res.* **2019,** *52* (9), 2516-2524.

Insert Table of Contents artwork here